

Gas distribution mapping of multiple odour sources using a mobile robot

Amy Loutfi†*, Silvia Coradeschi†, Achim J. Lilienthal†
and Javier Gonzalez‡

† *The Center for Applied Autonomous Sensor Systems, Örebro University, 701-82 Sweden.*

‡ *Department of System Engineering and Automation, University of Malaga, 29071 Malaga, Spain.*

(Received in Final Form: April 12, 2008. First published online: June 4, 2008)

SUMMARY

Mobile olfactory robots can be used in a number of relevant application areas where a better understanding of a gas distribution is needed, such as environmental monitoring and safety and security related fields. In this paper, we present a method to integrate the classification of odours together with gas distribution mapping. The resulting odour map is then correlated with the spatial information collected from a laser range scanner to form a combined map. Experiments are performed using a mobile robot in large and unmodified indoor and outdoor environments. Multiple odour sources are used and are identified using only transient information from the gas sensor response. The resulting multi-level map can be used as a representation of the collected odour data.

KEYWORDS: Mobile robots; Teleoperation; Mobile olfaction; Electronic nose; Gas mapping.

1. Introduction

The combination of gas sensors on mobile robots is useful for a number of application areas within safety, security and environmental inspection. Instead of using humans, a robot can be dispatched to areas of contaminous odours for inspection, or can provide continuous monitoring of an area with quantitative characterization of specific odours. In this paper, we address the integration of gas sensors onto a mobile robot for environmental inspection. The main contribution resides in the combination of a number of techniques in both static electronic olfaction and mobile robotics to create an odour map. The odour map shows the spatial layout of the environment, the presence of multiple gases and how these gases are distributed. All the sensor information is collected using a mobile robot equipped with an electronic nose, laser range-finder and a number of additional modalities to assist in navigation and interaction with its users. Such a system is intended to be used in applications where a user is working closely with the robotic system in order to gain deeper insight into the distribution of gases in various environments. An important additional contribution of this

paper is the consideration of large, unstructured and even partially outdoor environments.

1.1. Related work

The field of mobile olfaction currently has a number of key research directions including trail following,²³ localization of odour plume origin^{5,10} and mapping of odour distributions.^{12,24} Both two-dimensional and three-dimensional environments have been considered where the majority of experimental set-ups use single-odour sources. The majority of the mobile olfactory platforms use the TGS gas sensors⁶ as the main gas detection modality. Other types of sensors used include QMB and conducting polymer sensors.¹⁶ For experiments which consider trail following and navigation to the odour source by chemotaxis, restricted and controlled environments have been used. However, work considering gas distribution mapping and odour classification¹⁸ has considered unmodified environments for experimentation. This follows a recent trend to promote mobile olfactory robots for a number of real applications such as environmental monitoring¹⁹ and mine detection.²⁰ In order for olfactory robots to move towards this goal, it is essential to not only consider realistic environments, but also to use the full capability of current robotic research such as self-localization and mapping, and also consider the entire olfactory problem which includes both detection and identification of odours. Additional related work relevant to the methods applied in this paper is present in the technical sections.

1.2. Olfactory robot

Our experiments have been conducted using a service robot, called Sancho, which is intended to work within human environments as, for example, a conference or fair host (see Fig. 1a). It is constructed upon a pioneer 3DX mobile base whose structure has been devised to contain the sensorial system. The sensorial systems include a radial laser scanner, a set of 10 infrared sensors, a colour motorized camera and a pair of electronic noses placed at a low position in the frontal part of the robot (see Fig. 1b). All devices of Sancho are managed by a Pentium IV laptop computer (2.4 GHz) with wireless communication that connects Sancho to remote

* Corresponding author. E-mail: Amy.loutfi@tech.oru.se

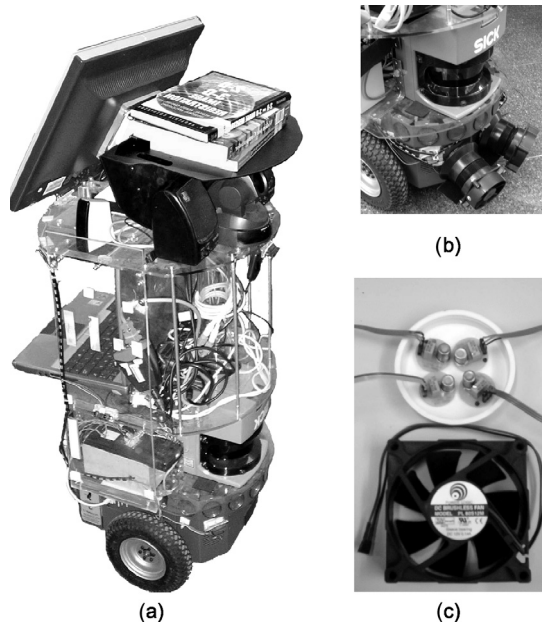


Fig. 1. Sancho, the service robot. (a) The original version of Sancho for delivery applications. (b) Partial view of the robot focusing on the two electronic noses mounted on Sancho for our experiments. (c) Each e-nose is composed of four gas sensors, a fan that provides a constant air flow and a retractable plastic tube (not shown in the picture) that directs the air flow to the sensors.

servers or to the internet, enabling, for instance, remote users to command and to control the robot.

Located on the front of Sancho approximately 11 cm from the floor are two electronic noses based on TGS Figaro technology. Each e-nose consists of four TGS sensors (TGS 2600 ($\times 2$), 2620, 2602). The design and choice of the sensors is such that the redundancy of the TGS 2600 sensor is advantageous for the mapping algorithm while the diversity of the sensor array is mainly used for the classification process. The four sensors are placed in a circular formation on a plastic backing (see Fig. 1c). The sensors are then placed inside a retractable plastic tube sealed with a CPU fan that provides a constant airflow into the tube (see Fig. 1b). The two e-noses are separated at a distance of 14 cm (measured from the centre of the circular backing). Each sensor's (s) position with respect to the centre of the robot is denoted by P_{xs} , P_{ys} , P_{zs} .

Readings from the gas sensors are collected by an on-board data acquisition system located on the frame of the robot and a sampling frequency of 1.25 Hz was used. Prior to experimentation, the sensor arrays for both e-noses were heated for approximately 30 min reaching temperatures between 300°C and 500°C, needed for proper operation. Metal oxide sensors exhibit some drawbacks worth noting, namely, a low selectivity, a comparatively high power consumption (caused by the heating device) and a weak durability. Furthermore, metal oxide sensors are subject to a long response time and an even longer decay time. However, this type of gas sensor is most often used for mobile noses because it is inexpensive, highly sensitive and relatively unaffected by changing environmental conditions like room temperature or humidity.

The software processing to create the odour maps consists of several components. The identification component used to

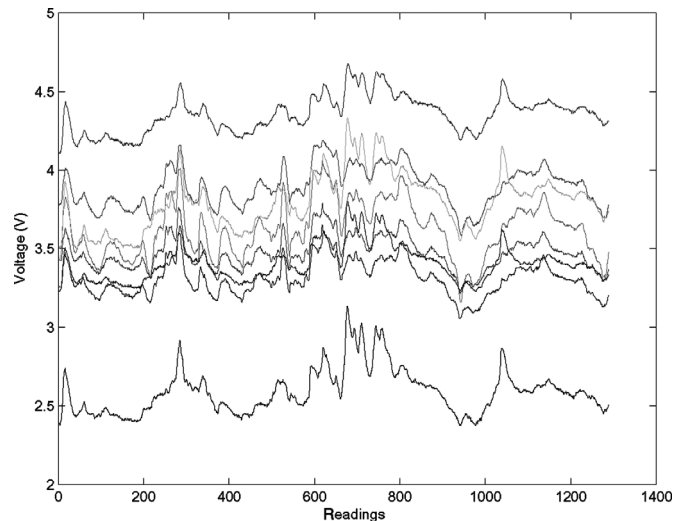


Fig. 2. Readings from the eight TGS sensors. Here the robot was moving in an inward spiral motion towards the centre of a room. An ethanol odour source consisting of a small cup filled with ethanol was located in the centre.

classify specific odourous types is described in Section 2. The computation of the gas distribution is described in Section 3 and the method used to combine these methods together with the laser range information is described in Section 4. Finally, experimental results showing the performance of the robot and the respective algorithms are given in Section 5.

2. Classification of Odours using Transient Response

Applications which deal with odour classification on static systems have primarily considered a three-phase sampling procedure, often extracting information about the steady-state response of the sensors. Input to the classification algorithm is then a comparison between a baseline and the steady state. Including recovery, a three-phase sampling can take anywhere from 2 to 5 min for a TGS sensor.

The challenge of odour classification with a mobile robot as it moves either towards or away from an odour source is that the concentration of an odourant is not constant. Also given the latency present in the sensor response prior to a steady state, it is not possible to rely on the power law to deduce the concentration as was presented in ref. [22]. Figure 2 shows a typical response from the electronic nose on Sancho, when patrolling an environment with an odour source. Here, it is reasonable to assume that while the robot is moving and current concentration values are unknown, the sensors are in a state of transition. Identification of an odour using only the transient information in a signal has been addressed previously for a number of static electronic nose systems.^{3, 7, 20} Of these methods, discrete wavelet transform (DWT) applied to the transient portion of a signal has shown to improve the classification performance when this transient information was included with steady state and recovery information.

To classify the signals collected from the robot as shown in Fig. 2, we first establish a training set consisting of transients for each odour character. The training data are collected with the electronic nose placed at a fixed distance

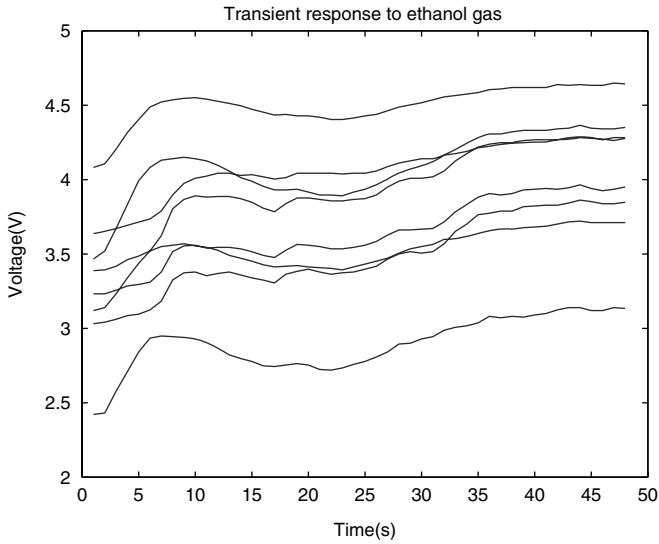


Fig. 3. Transient response of eight TGS gas sensors used to train the SVM.

from the odour source (approximately 20 cm) sampling the odour for a short period of time (between 20 and 30 s). The e-nose sampled each odour at 1.25 Hz, which is used throughout all experiments even with the robot. The training data set consists of $o = 1, \dots, N_o$ odour fingerprints. Each fingerprint consists of $s = 1, \dots, N_s$ sensor transients. Each sensor transient consists of $n = 1, \dots, N_t$ readings. The raw sensor response for sensor s to odour o at time t is denoted by $r_{o,s}(t_n)$. Using the signal shown in Fig. 3, a differential and fractional baseline manipulation is performed according to Eq. (1) to obtain $R_{o,s}$.

$$R_{o,s}(t_n) = r_{o,s}(t_n) - r_{o,s}(t_1). \quad (1)$$

The input signals to the training algorithm are decomposed into features using a set of DWTs formulated by Debauchies. The DWT creates a time scale representation of a digital signal using digital filtering techniques. It does so by analysing the signals at different frequency bands with different resolutions thereby decomposing the signal into a coarse approximation and detailed information. In terms of the gas sensors, this has been expressed as the decomposition of the transient's response according to the different rates of absorption caused by different odourants.⁴ Each $R_{o,s}$ is passed through a series of high pass filters ($g[t_n]$) to analyse the high frequencies, and low pass filters ($h[t_n]$) to analyse the lower frequencies according to

$$y_{\text{low}}[k] = \sum R_{o,s}[t_n]h[2k - t_n], \quad (2)$$

$$y_{\text{high}}[k] = \sum R_{o,s}[t_n]g[2k - t_n]. \quad (3)$$

Each iteration through a high pass and low pass filter represents one level of decomposition. After the first level, further decomposition is performed on the output of the low pass filter, subsequently downsampling by a factor of 2 from the previous level as illustrated in Fig. 4. The output of the high pass filter corresponds to the detail level coefficients,

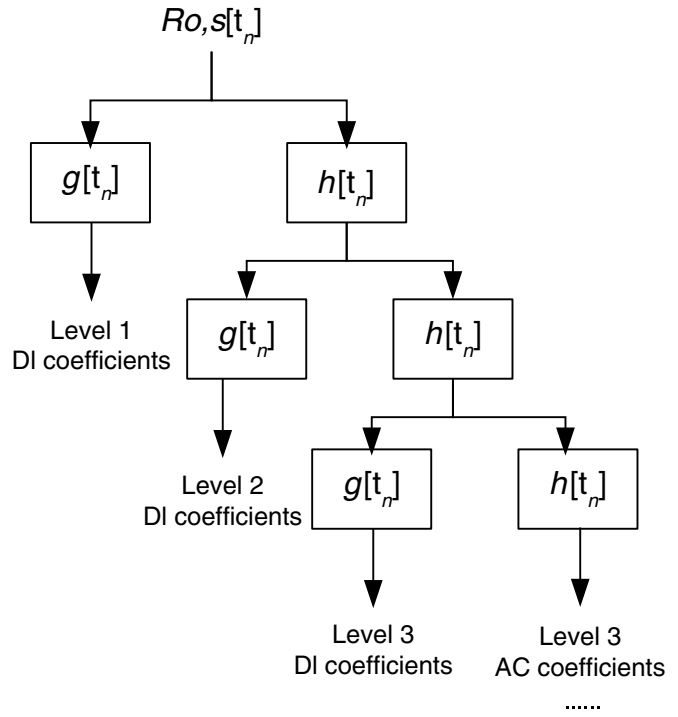


Fig. 4. The sub-band coding algorithm used to determine the wavelet coefficients for input to the SVM.

as frequencies most prominent in the original signal will appear as high amplitudes in that region including those particular frequencies. The resulting features are gathered by concatenating the detail coefficients, DL, for each level followed by the approximation coefficients, AC. Therefore each $R_{o,s}$ is expressed as

$$R_{o,s}^W = [DL_1 \dots DL_{N_w}, AC_1 \dots AC_{N_w}], \quad (4)$$

where N_w is the decomposition level. The total wavelet coefficients for each odour are first inputted into principal component analysis (PCA) and classified using a multi-class support vector machine (SVM) classifier. The multi-class SVM classifier is trained based on the binary SVM formulation and L2-soft margin penalisation of misclassifications. The quadratic programming task is optimized by the Mitchell–Demyanov–Malozemov algorithm using a Gaussian kernel function.

2.1. Training performance

To evaluate how well the system trains using only the transient information, we have sampled three odours, ethanol, acetone and plain air. These substances are then used as test substances for the experiments presented in Section 5, where the classification results to new samples acquired when the robot is moving are presented. To train the system, data are collected with the electronic nose (that is later used on the robot) placed at a fixed distance from the odour source (approximately 20 cm) sampling the odour for a short period of time (between 20 and 30 s). The e-nose sampled each odour at 1.25 Hz, also consistent with the sampling time later used with the robot. Approximately 50 transients of each odour were collected. The PCA results obtained after a DWT are shown in Fig. 5.

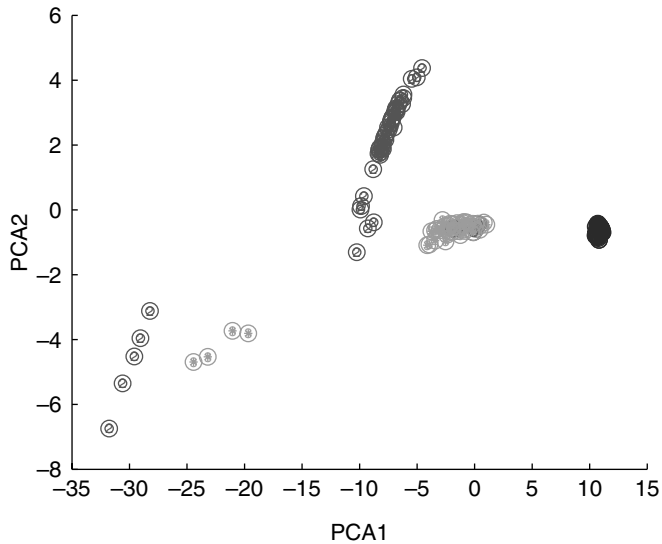


Fig. 5. Principal component analysis of the input $R_{o,s}^W$. Acetone is indicated in red, ethanol is indicated in green and plain air is indicated in blue.

The output of the SVM stabilizes after 200 iterations with a classification error of 7.5%. The matrix is non-symmetric and indicates a higher classification error of acetone samples. The source of error could be due to the fact that both ethanol and acetone samples are quite similar and the addition of a selective sensor could resolve the ambiguity (however, in this case a more symmetric confusion matrix would be generated). Another and more likely possibility is that at certain concentration levels within specific sample intervals, the transient reactions of acetone generate a similar response to those of ethanol (Table 1).

3. Gas Distribution Mapping

To be able to visualize the distribution of a particular gaseous compound, the classification algorithm is integrated with a gas concentration mapping (GDM) algorithm. Gas concentration mapping is a relatively new field in the area of olfactory robots, with some progress made with both single and multiple robots.^{8,11,19} The algorithm applied here is based on the algorithm presented in ref. [14] and further developed by the authors in ref. [13].

Due to fundamental differences between range sensing with a laser scanner and gas sensing with metal oxide sensors, traditional mapping techniques such as Bayesian estimation cannot be applied to the gas distribution mapping

problem in the same way as to estimate an occupancy grid map.

The main differences are, first, that the sensor readings do not allow to derive the instantaneous concentration levels directly. Metal oxide gas sensors are known to recover slowly after the target gas is removed (15–70 s)¹ and therefore perform temporal integration implicitly. Second, a snapshot of the gas distribution at a given instant contains little information about the distribution at another time due to the chaotic nature of turbulent gas transport. Turbulence generally dominates the dispersal of gas. As a consequence the instantaneous concentration field of a target gas released from a small static source is a chaotic distribution of intermittent patches with peak concentration values that are generally an order of magnitude higher compared to the time-averaged values.²¹ Third, in contrast to a typical range-finder sensor, a single measurement from a gas sensor provides information about a very small area because it represents only the reactions at the sensor's surface. Another consequence of the peculiarities of gas transport and gas sensing is that the gas sensor measurements do contain only little information about the current sensor location with respect to the time-averaged gas distribution.

In order to estimate a grid map that represents the time-averaged relative concentration of a detected gas, we use the kernel extrapolation gas distribution mapping method introduced by Lilienthal and Duckett.¹⁴ The main idea is to interpret the gas sensor measurements as noisy samples from a time-constant distribution. This implies that the gas distribution in fact exhibits time-constant structures, an assumption that is often fulfilled in unventilated and unpopulated indoor environments.²⁴ It is important to note that the noise is caused by the large fluctuations of the instantaneous gas distribution while the electronic noise on individual gas sensor readings is negligible.⁹

The kernel extrapolation gas distribution mapping method can cope to a certain degree with the temporal and spatial integration of successive readings that metal oxide gas sensors perform implicitly due to their slow response and long recovery time.¹⁵ In order to obtain a faithful representation of gas distribution despite the slow sensor dynamics ('memory effect'), the robot's path needs to fulfill the requirement that the directional component of the distortion due to the memory effect is averaged out. This can be achieved by driving the robot through the same coordinate from opposing directions.

The algorithm introduces the kernel width σ as a selectable parameter, corresponding to the size of the region of extrapolation around each measurement. This parameter allows the user to decide on a faster or more accurate map building process. Its value has to be set large enough to obtain sufficient coverage according to the path of the robot. Conversely, this means that for a larger kernel width a faster convergence can be achieved while preserving less details of the gas distribution in the map. Consequently, the selected value of the kernel width σ represents a trade-off between the need for sufficient coverage and the aim to preserve fine details of the mapped structures. Parameter selection and the impact of sensor dynamics are discussed in more detail in ref. [15].

Table 1. Confusion Matrix for Classification Performance of SVM.

Substance	Classifier		
	Ethanol	Acetone	Air
Ethanol	35	0	0
Acetone	12	54	0
Air	0	0	60

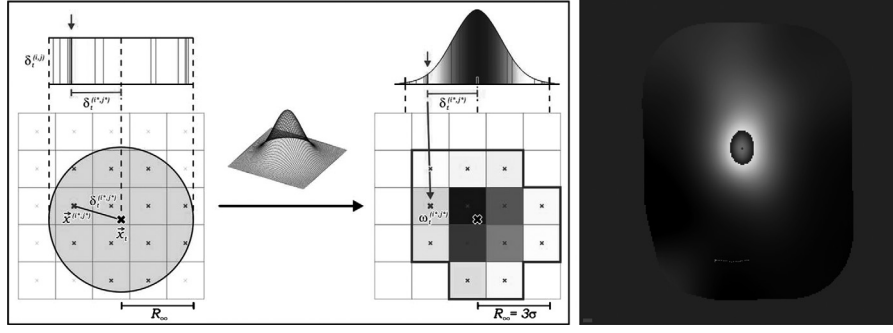


Fig. 6. Discretisation of the Gaussian weighting function onto the grid. (Left) For each grid cell within a cutoff radius R_{co} (represented by a circle) around the point of measurement \vec{x}_t , the displacement $\vec{\delta}_t^{(i,j)}$ is calculated. The corresponding distances are indicated for the 13 affected cells by the vertical lines drawn in the upper part. The weights $w_t^{(i,j)}$ are determined for all grid cells by applying a Gaussian function. ($\sigma = (1/3)R_{co}$). (Right) An example of a completed gas distribution map representing a 3 m \times 4 m area. The weights are indicated by shadings of grey (dark shadings correspond to high weights). A second colour and inverse shading scheme is used for concentration values exceeding 80%. A dotted line indicates the path of the robot.

Step-by-step explanation of kernel-based gas distribution mapping

The sensor readings are convolved using the univariate two-dimensional Gaussian function

$$f(\vec{x}) = \frac{1}{2\pi\sigma^2} e^{-\frac{\vec{x}^2}{2\sigma^2}}. \quad (5)$$

Then, the following steps are performed:

- In the first step the normalized readings r_t are determined from the raw sensor readings R_t as

$$r_t = \frac{R_t - R_{\min}}{R_{\max} - R_{\min}} \quad (6)$$

using the minimum and maximum (R_{\min} , R_{\max}) values of a given sensor.

- Then, for each grid cell (i, j) within a cutoff radius R_{co} , around the point \vec{x}_t where the measurement was taken at time t , the displacement $\vec{\delta}_t^{(i,j)}$ from the grid cell's centre $\vec{x}^{(i,j)}$ is calculated as

$$\vec{\delta}_t^{(i,j)} = \vec{x}^{(i,j)} - \vec{x}_t. \quad (7)$$

- Now the weighting $w_t^{(i,j)}$ for all the grid cells (i, j) is determined as

$$w_t^{(i,j)} = \begin{cases} f(\vec{\delta}_t^{(i,j)}) & : \delta_t^{(i,j)} \leq R_{co} \\ 0 & : \delta_t^{(i,j)} > R_{co} \end{cases}. \quad (8)$$

- Next, two temporary values maintained per grid cell are updated with this weighting; the total sum of the weights

$$M_x : W_t^{(i,j)} = \sum_{t'} w_{t'}^{(i,j)}, \quad (9)$$

and the total sum of weighted readings

$$M_{x_{z_{gas}}} : WR_t^{(i,j)} = \sum_{t'} r_{t'} w_{t'}^{(i,j)}. \quad (10)$$

- Finally, if the total sum of the weights $W_t^{(i,j)}$ exceeds the threshold value W_{\min} , the value of the grid cell is set to

$$c_t^{(i,j)} = WR_t^{(i,j)} / W_t^{(i,j)} \quad : \quad W_t^{(i,j)} \geq W_{\min}. \quad (11)$$

An example that shows how a single reading is convolved onto a 5 \times 5 grid map is given in Fig. 6. First, 13 cells are found to have a distance less than the cutoff radius from the point of measurement (Fig. 6, left). These cells are indicated in the right-hand side of Fig. 6 by a surrounding strong border. The weightings for these cells are then determined by evaluating the Gaussian function for the displacement values. In this example, the cutoff radius was chosen to be three times the width σ . The weights are represented by shadings of grey. Darker shadings indicate higher weights, which correspond to a stronger contribution of the measurement value r_t in the calculation of the average concentration value for a particular cell. As an example, a gas distribution map is shown in Fig. 6 (right).

4. Combination of the Maps

The GDM algorithm has been previously implemented with the assumption of homogeneous gas sensing types and the presence of a single odour source. Under these assumptions, Eq. (6) can be used with R_t which normalizes each of the sensor responses and correctly associates a shading based on the amplitude of the signal and the position of the sensor with respect to the centre of the robot. However, if a heterogeneous sensing array is used, the normalization of each sensor response will generate a misrepresentation of the concentration value needed for the GDM. This is due to the fact that sensors of different types react differently to the same odourant. So a TGS 2600 selective to alcohols will provide a strong reaction with high signal amplitude while a sensor of type TGS 2602 will provide little reaction at all. Therefore, in order to use the GDM algorithm as specified above, the original signal is first classified, collecting all sensor responses associated to a specific odour (denoted as odour filtering). The subsequent gas distribution map is then only evaluated for similar sensing types. Figure 7 summarizes the approach used in this work to combine the sensor modalities

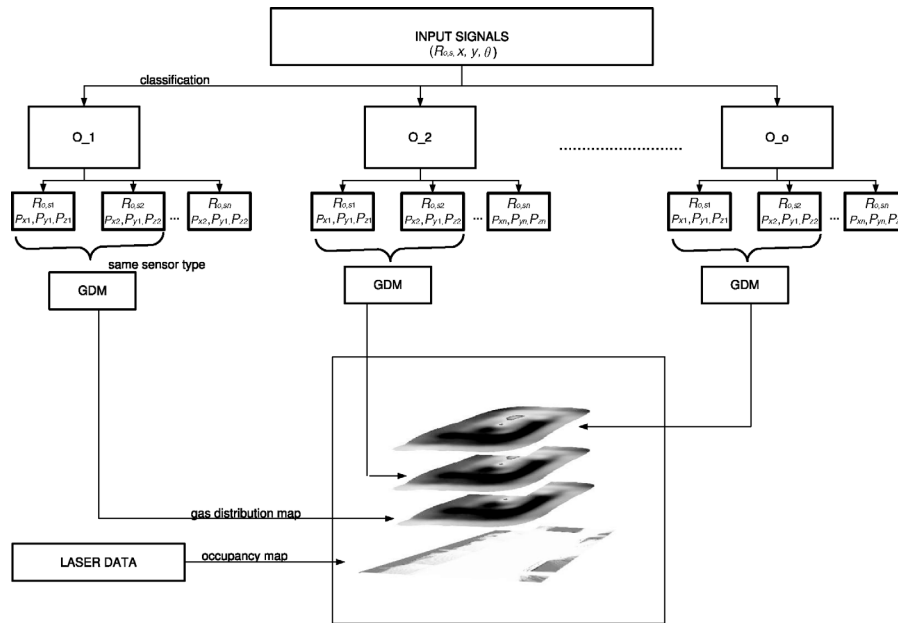


Fig. 7. Overview of the method used to integrate the classification algorithm with the GDM and finally the occupancy map. The signal is passed through a number of odour filters which identifies specific odour character using transient response. The identified signals are subsequently fed into the GDM which generates an image representing the gas distribution. Each image is then overlaid onto the spatial information obtained from the occupancy map.

in a singular map. The original signal is first processed through the odour filters, for each trained odour. This is done by parsing the signal into transients using a threshold to determine the change in the sensor response. The transients are identified and the position (x,y) and rotation (θ) of the robot corresponding to the signal response in the transient are stored. Signal responses between identified transients are associated to the odour id of the previous transient.

After classification the signal is separated according to each sensor. Similar sensor types are then collected and used in the GDM (e.g., all TGS 2600). Note that each sensor has a unique position on the robot with respect to the robot centre. The sensor position with respect to the robot, the signal response from the sensor and the corresponding position of the robot in the environment are used as input to the GDM. The GDM then combines the information from the sensors and this is done for each odour type.

Finally, in order to relate the gas distribution map to spatial information about the robot position and nearby obstacles, a localization module based on adaptive Monte Carlo particle filter was used. In this work, the map of the environment is generated *a priori* using a Rao-Blackwellized particle filter to address the simultaneous localisation and mapping (SLAM)

problem. The final map is provided to the system and the localization module returns the position and rotation estimate of the robot as it inspects the area. The position estimates are used as input to the GDM, and the laser data information and map are merged together with the output of the GDM and classification module. An alternative method to using a map generated *a priori* is to consider the SLAM problem in conjunction with the GDM process. This issue has been considered further in detail in ref. [13]; however, for the purpose of the experiments presented here and the validation of the classification performance the map is presupposed to be given *a priori*.

5. Experimental Results

5.1. Indoor experiments

In the first experiment, the robot is placed in a $3\text{ m} \times 4\text{ m}$ indoor room and performs a sweeping motion in the room as shown in Fig. 8 (left). Two odour types were used as sources, ethanol and acetone. In each trial only one of the odour types was present at a time and placed approximately in the centre of the room, marked by the square in the figure. Half of the

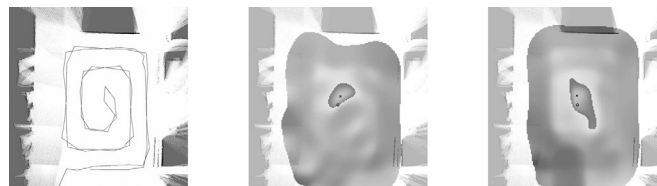


Fig. 8. Results from an inspection of an indoor room. (Left) The path taken from the robot overlaid on the occupancy map. (Middle) An example of the GDM obtained from an acetone source. (Right) An example of the GDM obtained from an ethanol source. Source position is indicated by a circle. Position of the maximum concentration is indicated by a cross.

Table 2. Classification performance and GDM performance in the Indoor Experiments.

Substance	Trials	Classification performance (%)	Distance to maximum (cm)
Ethanol	9	92.4 ± 9.8	5.67 ± 3.02
	4	88.3 ± 12.0	7.85 ± 2.02
Acetone	13	96.2 ± 5.67	9.55 ± 3.89
	5	94 ± 4.8	8.75 ± 2.68

collected experiments were performed autonomously by the robot, while the other half were performed with a human operator guiding the robot with a joystick. The purpose of the experiments was to evaluate the following: the performance of the classification algorithm to real data, the performance of the gas distribution map and finally the flexibility of the system to be teleoperated with a human present in the room. Table 2 summarizes the results from the experimental trials.

The classification performance is computed by testing the algorithm presented in Section 2 to new signals collected by the robot. Only two odour filters are used, acetone and ethanol. Although a third odour filter for the clean air could be included, it is omitted for visualization of the GDM. This is because the colouring scheme used in the GDM indicates regions of lower odour ‘concentration’ by darker shading. These regions also correspond to an absence of the specified odour (i.e., higher presence of clean air).

The performance criteria of the GDM are evaluated based on the proximity of the maximum odour concentration and its correlation to the actual source position. It should be noted that using this measure is not always accurate as air currents may cause the maximum concentration to drift from the odour source, as remarked by Lilienthal *et al.*¹⁷ However, in the absence of a true ground truth measure, this estimate has been adequate for the experiments. Furthermore, the examination of whether this estimate changes with regards to a human-operated sweep versus an autonomous sweep is indicative of the validity of the human-operated investigation. In Fig. 8, a typical sweep is shown for both different gas source types, with $\sigma = 25$ cm and considering only the response from the TGS 2600 sensors for the map creation.

The classification performance is relatively stable throughout the different test runs and at varying distances from the odour source. This can be attributed in part to the type of the environment and the type of odour sources being used. Since the robot in all cases is moving relatively slowly to reduce the effect of the robot’s movements on the gas distribution, an experimental sweep takes approximately 30–40 min. Furthermore, the high volatility of the gas sources causes the gas molecules to quickly distribute in the indoor room.

5.2. Semi-outdoor experiments

Using the same sources, a second experiment was performed in a larger and less structured environment with both sources present at the same time but separated by a large distance to minimize the effect of mixing. In Fig. 9 (left) the laser scan of a large partially indoor environment located at Malaga University, Spain, was used. This environment is composed of four connecting corridors. The upper corridor is approximately $20 \text{ m} \times 2.5 \text{ m}$ and its partially outdoor corridor used as a passageway. It connects to the lower corridor which is located indoors via two smaller corridors (right and left) in the figure. The odour source positions are indicated by a small circular region. The ethanol is placed in the indoor lower corridor and the acetone in the upper corridor. The path of the robot, this time guided by a human operator, is indicated in the right-hand side of the figure.

The final gas distribution map is shown in Fig. 10 (left). To distinguish between the two different sources, two different shading colours are used for concentration values exceeding 80% of the maximum signal amplitude. The distance between the concentration maximum is 5.6 cm for the ethanol source and 48.2 cm for the acetone source. It is expected that since the acetone source is placed in a partially outdoor



Fig. 9. (Left) Occupancy map of the long corridor experiment with source positions; acetone source is located in the upper corridor and the ethanol source is located in the lower (indoor) corridor. (Right) Path of robot guided by the human user, a series of two passageways connects the lower and upper corridor to each other.



Fig. 10. The gas distribution map of the corridor and the largest map made. (Left) The presence of the two sources is indicated using different colouring schemes, green represents the ethanol and red represents the acetone source. Only concentrations exceeding 80% of the maximum for each odour are displayed in colour. (Right) No classification is performed and therefore only one colour is used to represent the spread of the odour. Without classification the ethanol source is under-represented.

Table 3. Classification Performance in long corridor with two odour sources.

Substance	5–20 cm	20–50 cm	50–100 cm	100–150 cm	150–250 cm	250–350 cm
Ethanol	100%	98.2%	98.2%	87.5%	85.5%	86.5%
Acetone	100%	97.0%	100%	95.4%	96.3%	93.2%

environment, turbulent airflow may have carried or displaced gaseous molecules from the source location causing not only the maximum measured concentration to be far from the source location but also a much more dispersed plume to be present. For comparison, in Fig. 10 (right), a gas distribution map is generated using the entire signal without consideration of the odour classification but only averaging the signals from the same sensor type. The main difference here is that the spread of the acetone gas is much more prominent especially in comparison to the ethanol source. This result is expected if acetone signals generally produce a strong reaction for the TGS 2600 sensor. Therefore, by using the classification algorithm as presented in the scheme shown in Fig. 7 the maximum concentration of each odour is equally represented in the map as opposed to only capturing the maximum reaction of the entire signal. This facilitates the detection of multiple odours despite a biased selectivity of the sensor.

Examining the classification performance is again another challenge given the presence of two odours and the absence of knowledge about the particularities of odour mixtures and its effect on the response from the sensors. To avoid mixing, the sources have been placed at a far distance from each other. The final classification performance is presented in terms of the distance of the robot to the actual source position. Table 3 summarizes the classification performance and shows that as the distance from the source increases, the classification performance degrades. If one would test with the two sources closer together, the SVM would need to be trained on different possible mixtures of the odours.

6. Conclusion

In this work, we presented a robotic system which combines techniques in static olfaction, and mobile robotics to create a holistic representation of a gas distribution that includes classification and spatial information. The experimental

results show that the robot performs equally well when operated autonomously as when operated by a human user. Experiments were performed with reasonable results in large and unmodified environments, this combined with the importance of including classification information of an odour are significant contributions towards real-world applications for olfactory robots. A video demonstration of the experiments presented in this paper is available at <http://www.aass.oru.se/~ali/malaga.html>.

A number of remaining challenges are still worth noting. Firstly, classification of odour mixtures is still a difficult problem particularly for systems which are not previously trained to detect the specific mixture. A better understanding of the response from the gas sensors and in particular when used on a mobile robot is needed. Another significant challenge is the problem of ground truth evaluation which although clearly present for the gas distribution evaluation is also present for the classification problem. A possible direction for future work may be to consider multiple robots working in the same environment, but using different techniques for measuring gas distribution. A secondary alternative may be to combine information from different sensors, such as information about how odours propagate around obstacles and wind information in order to verify the correlation to the gas sensing results.

Acknowledgements

This work has been supported by the Swedish Research Council (Vetenskapsrådet). The authors would also like to thank Jose Luis Blanco and Cipriano Galindo of University of Malaga for providing valuable support during the experimental implementation.

References

1. K. J. Albert and N. S. Lewis, "Cross reactive chemical sensor arrays," *Chem. Rev.* **100**, 2595–2626 (2000).

2. S. Badia, U. Bernardet, A. Guanella, P. Pyk and P. Verschure, "A biologically based chemo-sensing uav for humanitarian demining," *Int. J. Adv. Rob. Syst.* **4**(2), 187–198 (2007).
3. C. Distante, M. Leo, P. Siciliano and K. Persaud, "On the study of feature extraction methods for an electronic nose," *Sens. Actuators B* **87**, 274–288 (2002).
4. C. Distante, M. Leo, P. Siciliano and K. Persaud, "Olfactory sensory system for odour-plume tracking and localization," *Sensors* **1**, 418–423 (2003).
5. T. Duckett, M. Axelsson and A. Saffiotti, "Learning to Locate an Odour Source With a Mobile Robot," *Proceedings of the IEEE International Conference on Robotics and Automation (ICRA'2001)*, Seoul, Korea (2001).
6. Figaro Gas Sensor: Technical Reference, 1992. <http://www.figaro.com>.
7. R. Gutierrez-Osuna, A. Gutierrez-Galvez and N. U. Powar, "Transient response analysis for temperature modulated chemoresistors," *Sens. Actuators B: Chem. B* **93**(1–3), 57–66 (2003).
8. A. T. Hayes, A. Martinoli and R. M. Goodman, "Distributed odor source localization," *IEEE Sens.* **2**(3) 260–273 (2002).
9. H. Ishida, A. Kobayashi, T. Nakamoto and T. Moriizumi, "Three-dimensional odor compass," *IEEE Trans. Rob. Automat.* **15**(2), 251–257 (Apr. 1999).
10. H. Ishida, T. Nakamoto and T. Moriizumi, "Remote sensing of gas/odor source location and concentration distribution using mobile system," *Sens. Actuators B* **49**, 52–57 (1998).
11. H. Ishida, T. Yamanaka, N. Kushida, T. Nakamoto and T. Moriizumi, "Study of real-time visualization of gas/odor flow images using gas sensor array," *Sens. Actuators B* **65**, 14–16 (2000).
12. A. Lilienthal and T. Duckett, "Creating Gas Concentration Gridmaps With a Mobile Robot," *Proceedings of the 2003 IEEE/RSJ International Conference on Intelligent Robots and Systems (IROS 2003)*, IEEE Press, Las Vegas, USA (2003).
13. A. Lilienthal, A. Loutfi, J. Blanco, C. Galindo and J. Gonzalez, "A Rao-Blackwellisation Approach to GDM-SLAM - Integrating SLAM and Gas Distribution Mapping," *Proceedings of the 3rd European Conference on Mobile Robots (ECMR)*, Freiburg, Germany (2007), pp. 126–131.
14. A. J. Lilienthal and T. Duckett, "Creating Gas Concentration Gridmaps with a Mobile Robot," *Proceedings of IEEE IROS*, Las Vegas, USA (2003), pp. 118–123.
15. A. J. Lilienthal and T. Duckett, "Building gas concentration gridmaps with a mobile robot," *Rob. Autonom. Syst.* **48**(1), 3–16 (Aug. 2004).
16. A. J. Lilienthal, A. Loutfi and T. Duckett, "Airborne chemical sensing with mobile robots," *Sensors* **6**, 1616–1678 (Oct. 2006). Available at <http://www.mdpi.org/sensors/papers/s6111616.pdf>
17. A. J. Lilienthal, H. Ulmer, H. Frohlich, F. Werner and A. Zell, "Learning to Detect Proximity to a Gas Source with a Mobile Robot," *Proceedings of the IEEE/RSJ International Conference on Intelligent Robots and Systems (IROS)*, Sendai, Japan, (Sep. 28–Oct. 2, 2004) pp. 1444–1449.
18. A. Loutfi, S. Coradeschi, L. Karlsson and M. Broxvall, "Object recognition: A new application for smelling robots," *Rob. Autonom. Syst.* **52**, 272–289 (2005).
19. L. Marques, A. Martins and A. Almeida, "Environmental monitoring with mobile robots," *Proceedings of the IEEE/RSJ International Conference on Intelligent Robots and Systems (IROS)*, Edmonton, Canada (2005) pp. 3624–3629.
20. L. Marques, U. Nunes and A. de Almeida, "Olfaction-based mobile robot navigation," *Thin Solid Films* **418**, 51–58 (2002).
21. P. J. W. Roberts and D. R. Webster, "Turbulent Diffusion," *In: Environmental Fluid Mechanics—Theories and Application* (H. Shen, A. Cheng, K.-H. Wang, M. Teng and C. Liu, eds.) (ASCE Press, Reston, Virginia, 2002).
22. O. Rochel, D. Martinez, E. Hugues and F. Sarry, "Stereo-Olfaction With a Sniffing Neuromorphic Robot Using Spiking Neurons," *16th European Conference on Solid-State Transducers—EUROSENSORS*, Prague, Czech Republic (Sep. 2002). Available at <http://www.loria.fr/publications/2002/A02-R-139/A02-R-139.ps>
23. R. Russell, D. Thiel and A. Mackay-Sim, "Sensing Odour Trails for Mobile Robot Navigation," *IEEE International Conference on Robotics and Automation (ICRA 1994)*, San Diego, USA (1994), pp. 2672–2677.
24. M. R. Wandel, A. J. Lilienthal, T. Duckett, U. Weimar and A. Zell, "Gas Distribution in Unventilated Indoor Environments Inspected by a Mobile Robot," *Proceeding of IEEE ICAR*, Coimbra, Portugal (2003), pp. 507–512.